ACTA IMEKO
ISSN: 2221-870X
March 2020, Volume 9, Number 1, 1 - 7

3D-printers dielectric materials characterization at microwave frequencies

Andrea Alimenti[1], Kostiantyn Torokhtii[1], Nicola Pompeo[1], Emanuele Piuzzi[2] and Enrico Silva[1]

[1] *Dipartimento di Ingegneria, Università degli Studi Roma Tre, 00146 Roma, Italy*
[2] *Dipartimento di Ingegneria dell'Informazione, Elettronica e Telecomunicazioni, Sapienza Università di Roma, Roma, Italy*

ABSTRACT
3D-printer materials are becoming increasingly more appealing also for high frequency applications. Thus, the electromagnetic characterization of these materials is an important step in order to evaluate their applicability in new technological devices. We present a measurement method for the complex permittivity evaluation based on a dielectric loaded resonator (DR). Comparing the quality factor Q of the DR with a disk-shaped sample placed on a DR base with Q obtained when the sample is substituted with an air gap, allows a reliable loss tangent determination.

Section: RESEARCH PAPER

Keywords: microwave characterization, loss tangent, 3D-printer materials, dielectric resonator

Citation: Andrea Alimenti, Kostiantyn Torokhtii, Nicola Pompeo, Emanuele Piuzzi and Enrico Silva, Microwave characterization of 3D-printer dielectric materials, Acta IMEKO, vol. A, no. B, article C, Month Year, identifier: IMEKO-ACTA-A (Year)-B-C

Section Editor: name, affiliation

Received month day, year; **In final form** month day, year; **Published** Month Year

Corresponding author: Andrea Alimenti, e-mail: andrea.alimenti@uniroma3.it

Corresponding author: Paul P. L. Regtien, e-mail: paul@regtien.net

1. INTRODUCTION

In the last years the fast development and improvement of 3D-print techniques have strongly affected many human activities [1-5]. Printed materials are also involved in high frequency applications as telecommunication technologies up to microwave frequencies [6-12]. Thus, a reliable and handy electromagnetic (e.m.) characterization is increasingly requested [13].

In this work we present the microwave characterization of plastic materials for 3D-printers with a resonant perturbative technique. The physical quantity under investigation is the permittivity ε, which is defined as the quantity (in the more general case a tensor) which describes the proportionality between the electric displacement vector $\boldsymbol{D}$ and the electric field strength vector $\boldsymbol{E}$ in a medium, $\boldsymbol{D} = \varepsilon_0 \boldsymbol{\varepsilon} \cdot \boldsymbol{E}$ with ε_0 the vacuum permittivity. In our case we consider isotropic and homogeneous materials in their linear regime, then $\boldsymbol{\varepsilon} = \tilde{\varepsilon}$ is a scalar quantity which does not depend on the position. The scalar complex relative permittivity is defined as $\tilde{\varepsilon} = \varepsilon' - \mathrm{i}\varepsilon''$, where the real part ε' is a measure of the energy storage properties of the medium while the imaginary part ε'' is related to the e.m. losses and $\mathrm{i} = \sqrt{-1}$. Since $\tilde{\varepsilon}$ is a complex quantity, it is often represented on the complex plane, where the angle δ between $\tilde{\varepsilon}$ and the real axis is known as loss angle. Thus, the ratio $\varepsilon''/\varepsilon' = \tan\delta$ is called the loss tangent.

We propose in this work a microwave (~ 12.9 GHz) measurement method based on a resonant technique. We show that a specially designed dielectric loaded resonator (DR) can be used to measure $\tilde{\varepsilon}$ by placing the dielectric sample on one of its flat bases, without the need for disassembling and reassembling the whole structure for each measurement, thus reducing the uncertainties involved. DRs are well known for their high sensitivity [14], but also for the poor measurement repeatability [15-16] in particular for what concerns the resonant frequency. Thus, a closed structure can be particularly useful to characterize samples by reducing systematic errors inevitably introduced by each mounting procedure. Moreover, since it is not necessary to reassemble the resonator for each measurement, the measurement time is reduced.

We substituted a part of the volume of the resonating structure with the dielectric material under study. Comparison of the changes induced by the sample insertion of the unloaded quality factor Q and the resonant frequency f_0 can be used to evaluate the electric/magnetic properties of the sample. If the changes on the distribution of the electromagnetic (e.m.) field caused by the insertion of the sample are "small", the resonant medium perturbation method [14] can be used.

Dielectric printed materials are already used for high frequency applications and some works explored their dielectric permittivity. Noticeable is the result obtained in [18] where acrylonitrile butadiene styrene (ABS) doped with different quantities of $BaTiO_3$ microparticles, allowed to obtain $2.6 < \varepsilon' < 8.7$ and $0.005 < \tan\delta < 0.027$, thus opening the possibility to engineer these materials for specific needs. The measurements were performed at 15 GHz with a split post dielectric resonator obtaining $u(\tan\delta)/\tan\delta \sim 0.4\,\%$. The split post resonator is a very sensitive measurement instrument but with critical issues related to the assembly procedure [14]. Our resonator works at a similar frequency (~ 12.9 GHz), with a somewhat reduced sensitivity with respect to a split post resonator, but with much improved ease of operation, a useful feature in view of routine measurements.

In Sec. 2 we present the measurement method and system. Then, in Sec. 3 a detailed uncertainties analysis is shown. In Sec. 4 we present the experimental results and, in Sec. 5, we compare the obtained results to those given by a standard waveguide transmission/reflection method and to other relevant scientific works [13], [17], [18]. A short summary is presented in Sec 6.

2. DESCRIPTION OF THE METHOD

We use a special configuration of a dielectric loaded resonator in Hakki-Coleman [19] configuration, designed to guarantee enhanced measurement repeatability at room temperature. The two physical quantities that characterize the response of the resonator are the unloaded quality factor Q and the resonant frequency f_0. Q is defined as $Q = \omega_0 W/P$, where W is the energy stored into the resonator at the resonant angular frequency $\omega_0 = 2\pi f_0$ and P the power dissipated at the same frequency. Thus, as we will show below, we can obtain the information about the dielectric losses of the material under study (i.e. $\tan\delta$), from the Q measurement.

P is the sum of all the power losses $P = P_S + P_\Omega + P_V$, where we indicate with the subscripts S, Ω, V the quantities related respectively to the sample, to the metal surfaces and to all the other dielectric materials inside the resonator volume. Hence:

$$\frac{1}{Q} = \frac{P_S + P_\Omega + P_V}{\omega_0 W} = \frac{1}{Q_S} + \frac{1}{Q_\Omega} + \frac{1}{Q_V}, \tag{1}$$

with:

$$\frac{1}{Q_S} = \frac{\int_{V_S} \varepsilon_S'' \varepsilon_0 |\mathbf{E}|^2 \mathrm{d}V}{2W} = \left[\frac{\varepsilon_S' \int_{V_S} \varepsilon_0 |\mathbf{E}|^2 \mathrm{d}V}{2W}\right] \frac{\varepsilon_S''}{\varepsilon_S'} = \eta_S \tan\delta, \tag{2}$$

$$\frac{1}{Q_\Omega} = \sum_i \frac{\int_{S_i} R_i |\boldsymbol{H}_\tau|^2 \mathrm{d}S}{2W} = \sum_i \frac{R_i}{G_i}, \tag{3}$$

$$\frac{1}{Q_V} = \frac{\int_{V_V} \varepsilon_V'' \varepsilon_0 |\boldsymbol{E}|^2 dV}{2W} = \eta_V \tan\delta_V\,, \tag{4}$$

where $\boldsymbol{E}$ is the electric field and $\boldsymbol{H}_\tau$ is the magnetic field tangential to the i-th metallic surface S_i with surface resistance R_i and geometrical factor G_i. η_S and η_V are the filling factors of the sample and of the dielectric elements inside the resonator respectively. Thus:

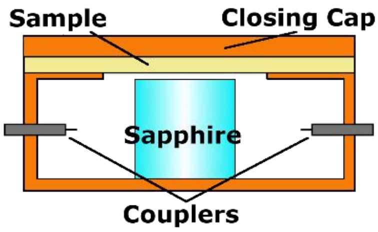

Figure 1. Sketch of the dielectric loaded resonator (not to scale).

$$\frac{1}{Q} = \eta_S \tan\delta_S + \sum_i \frac{R_i}{G_i} + \eta_V \tan\delta_V \tag{5}$$

Since W and the field configuration depend on ε' of all the dielectric elements inside the resonator, both η and G are functions also of ε_S'. Thus, to evaluate $\tan\delta_S$ of the dielectric sample placed in the resonator from Eq. (5), ε_S' must be measured. To this aim, one can exploit f_0 of the resonator as a second measurand. However, it is known that the absolute value of f_0 is strongly affected by many intrinsic (e.g. the electromagnetic properties of the elements inside the resonator) and extrinsic (e.g. temperature, pressure, humidity) factors, so that it is very difficult to exploit it in practice. However, the variation $\Delta f_0/f_{0,ref}$ of f_0, with respect to the reference value $f_{0,ref}$, due to the changes in one or more parameters is much more reliable [14]. In our case, we measure Δf_0 caused by the insertion of the dielectric sample. Then, with electromagnetic simulations we calculate Δf_0 as a function of ε_S' until the simulated and measured Δf_0 coincide. Thus, ε_S' is evaluated with the aid of e.m. simulations of the resonator.

After that ε_S' is evaluated, the factors η and G in Eq. (5) can be analytically or numerically (with simulators) calculated. Then, Eq. (5) can be inverted to obtain $\tan\delta_S$ from Q measurements if all the R_i and $\tan\delta_V$ of the resonator are known from previous measurements or calibration procedures.

It must be mentioned that the unloaded Q in Eq. (5) differs in principle from the measured Q_l because of the coupling of the resonator with the external lines. However, with very small coupling (i.e. $P_{ext}/P < 0.01$ with P_{ext} the losses in the external transmission lines), as in our working condition, one has $Q_l \sim Q$ and $u(Q) \sim u(Q_l)$ [14].

The use of Eq. (5) can give unacceptably large uncertainties since at microwave frequencies, the accuracy with which all the quantities in Eq. (5) are known is poor if compared to dc or low frequency measurements. In fact, in our case, we have $R = 92\ \mathrm{m\Omega}$ with $u(R)/R \sim 15\,\%$ and $\tan\delta_V = 4\cdot 10^{-5}$ with $u(\tan\delta_V)/\tan\delta_V \sim 50\,\%$.

In order to reduce the contribution of these uncertainties on $\tan\delta_S$, we propose to use a perturbative approach. The difference $\Delta(Q^{-1})$ between the measured quality factors Q_S^{-1} and Q_A^{-1}, obtained with the sample into the resonator (subscript S) or with a gap of air in its place (subscript A) respectively, can be written as:

$$\Delta(Q^{-1}) = \eta_S \tan\delta_S + \sum_i R_i \Delta(G_i^{-1}) + \Delta(\eta_V)\tan\delta_V, \tag{6}$$

where it is clear that the smaller $\Delta(G_i^{-1})$ and $\Delta(\eta_V)$ are, then the smaller the uncertainties on R_i and $\tan\delta_V$ contributions are.

2.1. Measurement system and procedure

The resonator used for this study is depicted in Figure 1. The sapphire single crystal is a cylinder (height $h = 5.0 \pm 0.1$ mm, diameter $\varnothing = 8.0 \pm 0.1$ mm). A K-type coaxial transmission line, ended with coupling loops, is used to excite and sense (in transmission mode) the e.m. field configuration into the resonator. The dielectric samples are supported by a brass mask with a central hole $\varnothing = (13.00 \pm 0.01)$ mm and closed with a brass cap in order to prevent energy radiation as depicted in Figure 1. The DR is excited in the TE_{011} mode thus the $\boldsymbol{E}$ field is oriented parallel to the bases of the resonator. It is important to underline the orientation of the $\boldsymbol{E}$ field because the layered deposition techniques, typical of most of the 3D-printers, can generate anisotropic effects on the e.m. properties of the printed samples. It was measured a uniaxial anisotropy factor of almost 7 % on ε' at 40 GHz on polylactide (PLA) samples with waveguide reflection method [17]. In the method presented here the $\boldsymbol{E}$ field is almost parallel to the deposition layers of the sample, thus our results probe the direction along the layer deposition, without significant mixing of the perpendicular component.

The resonator transmission scattering complex parameter S_{12}, from which Q and f_0 are evaluated, is measured with an Anritsu 37269D Vector Network Analyzer (VNA), with the following procedure:

- The VNA is calibrated with SOLT method and the 12-errors parameters are applied to the frequency range in which the measurements are performed;
- The transmission scattering parameter $S_{12}(f)$ is acquired with 1601 points evenly distributed in a frequency range width $7\Delta f_{-3dB}$, where Δf_{-3dB} is the width of the resonance curve at half power. Each data point is averaged with 10 acquisitions to reduce the noise contribution;
- The absolute value of the acquired points $|S_{12}(f)|$, with their uncertainty $u\big(S_{21}(f)\big)$, given by the VNA after the calibration [21], are fitted to the Fano resonance curve [22, 23]:

$$|S_{12}(f)| = \left| \frac{S_{12}(f_0)}{1 + 2\mathrm{i}Q\dfrac{f - f_0}{f_0}} + S_c \right|, \tag{7}$$

  where the complex constant S_c represents the cross-coupling contribution. For each resonance curve, Q and f_0 are evaluated with their uncertainties $u(Q)$, $u(f_0)$. The uncertainties on the fitting parameters are obtained by standard statistical methods starting from the fitting residuals variance σ_R^2 [20];
- For each mounting 10 resonance curves are acquired. Then, the mean values of Q and f_0 are evaluated with their standard deviation: $u(Q)/Q \sim 0.05\,\%$ and $u(f_0)/f_0 \sim 1$ ppm;
- For each sample 5 mountings are performed disassembling and resetting the sample in its position. Then, the mean value of Q and f_0 with their standard deviation are evaluated. The final uncertainties $u(Q)/Q \sim 1\,\%$ and $u(f_0)/f_0 \sim 20$ ppm are mainly due to the assembling repeatability.

3. UNCERTAINTIES ANALYSIS

In this section we explore the behaviour of the measurement technique in the whole sample parameters space in order to establish the best working condition and its boundaries as a function of ε_s', $\tan\delta_s$ and sample thickness t.

First, we analyse the sensitivity of the resonator to $\tan\delta_s$ variations. The sensitivity is evaluated from Eq. (5), as:

$$c = \frac{\partial Q}{\partial \tan\delta_S} = -\frac{\eta_S}{(\eta_S \tan\delta_S + l_r)^2} = -\eta_S Q^2, \tag{8}$$

with $l_r = \sum_i \frac{R_i}{G_i} + \eta_V\, tan\,\delta_V$ which, as a first approximation, in this analysis is assumed to be independent from the sample properties: in the small perturbation limit the changes in the e.m. field configuration due to the sample are small and practically negligible, thus the conduction/volume losses given by the resonator components do not change appreciably. In our case, $l_r \sim 5000 = Q_A^{-1}$.

In Figure 2, $|c(\tan\delta_s, \eta_s)|$ is reported for $10^{-5} < \tan\delta_s < 10^{0}$ and $\eta_s = \{10^{-4}, 10^{-3}, 10^{-2}, 10^{-1}\}$. We can notice a different $\log|c|$ slope m at high $\tan\delta_s$ values ($m = -2$) and at low $\tan\delta_s$ ($m = 0$) in the log-log plot (Figure 2). The $m = -2$ behaviour is given by the losses inside the dielectric samples when these are prevailing: $\eta_s\, tan\,\delta_s \gg l_r$, then from Eq. (8) $c \to -\eta_s^{-1}(\tan\delta_s)^{-2}$. Instead, when $\eta_s \tan\delta_s \ll l_r$, $c \to -\eta_s {l_r}^{-2}$ thus c is no more dependent on $\tan\delta_s$. As expected, the bigger η_s the higher $|c|$ as long as the sample losses are small. Thus, for low $\tan\delta_s$ samples, a higher η_s is preferable while at higher $\tan\delta_s$, a lower η_s gives better performances.

At a fixed $\tan\delta_s$ value the maximum of the sensitivity is obtained at the crossover of $|c|$ (see Figure 2) thus $\eta_s = \eta_{s,opt} = l_r / \tan\delta_s$ and $|c|_{max} = (4 l_r \tan\delta_s)^{-1}$. $\eta_{s,opt}$ is the optimum sample filling factor which gives the maximum sensitivity on Q measurements. Thus, the geometry of the samples under investigation can be adjusted in order to fulfil the $\eta_{s,opt}$ requirement. In our case, the expected $\tan\delta_s \sim 10^{-2}$, thus from Figure 2 $\eta_{s,opt} \sim 10^{-2}$.

The loss tangent measure uncertainty $u(\tan\delta_s)$ is evaluated as follows [20]:

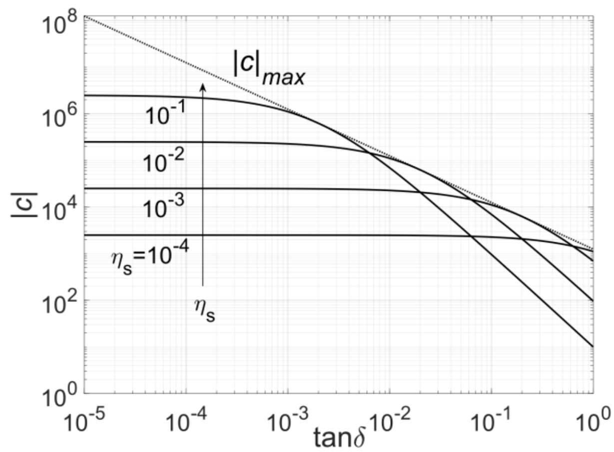

Figure 2. Solid lines: the absolute value of resonator sensitivity $|c|$ as a function of the sample $tan\,\delta_s$ and filling factor η_s. Dotted line: the maximum sensitivity $|c|_{max}$ reachable for every $tan\,\delta_s$ value.

$$
\begin{aligned}
u^2(\tan\delta_S) &= \frac{1}{\eta_S^2}\Bigg[\Big(u\big(\Delta(Q^{-1})\big)\Big)^2 + \sum_i \big(\Delta(G^{-1})u(R_i)\big)^2 \\
&+ \sum_i \Big(R_i u\big(\Delta(G^{-1})\big)\Big)^2 + \big(\tan\delta_V u\big(\Delta(\eta_V)\big)\big)^2 \\
&+ \big(\Delta(\eta_V)u(\tan\delta_V)\big)^2 + (\tan\delta_S u(\eta_S))^2\Bigg],
\end{aligned} \tag{9}
$$

with:

$$
u^2\big(\Delta(Q^{-1})\big) = \left(\frac{u(Q_S)}{Q_S^2}\right)^2 + \left(\frac{u(Q_A)}{Q_A^2}\right)^2, \tag{10}
$$

$$
\begin{aligned}
u^2\big(\Delta(G^{-1})\big) &= \left(\frac{u(G_{i,S})}{G_{i,S}^2}\right)^2 + \left(\frac{u(G_{i,A})}{G_{i,A}^2}\right)^2 \\
&- 2r_G \frac{u(G_{i,S})u(G_{i,A})}{G_{i,S}^2 G_{i,A}^2},
\end{aligned} \tag{11}
$$

$$
u^2\big(\Delta(\eta_V)\big) = u^2(\eta_{V,S}) + u^2(\eta_{V,A}) - 2r_\eta u(\eta_{V,S})u(\eta_{V,A}). \tag{12}
$$

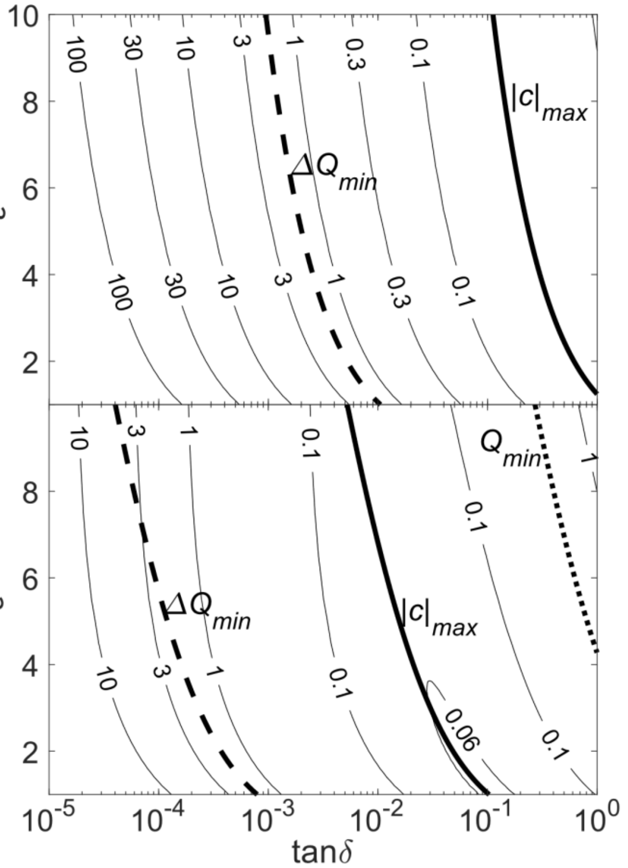

Figure 3. Relative loss tangent uncertainty $u(tan\,\delta_S)/\,tan\,\delta_s$ contour plot in the plane $(\varepsilon', \tan\delta)$ for sample of thickness $t = 0.5$ mm (a) and $t = 1.5$ mm (b). The thicker solid line represents the points of maximum sensitivity $|c|_{max}$ as evaluated from Figure 2. The dashed line corresponds to the minimum quality factor appreciable variation $\Delta Q_{min} = Q_A - Q_S \sim 40$ and the dotted on to the minimum evaluable $Q_{S,min} \sim 100$.

The correlation factors r_G and r_η are supposed to be almost 1 since the evaluation of G_i and η_V is performed with the same algorithm and with the same settings. Instead, the Q measurements are not strongly correlated since the different mountings can give different uncorrelated error contributions.

Then, $u(\tan\delta_s)$ is explored in the $(1 < \varepsilon' < 10,$ $10^{-5} < \tan\delta_s < 10^0, 0.5\text{ mm} < t < 2\text{ mm})$ space to establish the operative limits of this technique. $u(\tan\delta_s)$ is evaluated with Eq. (9) with geometrical G and filling η factors obtained through e.m. simulations. We verified with e.m. simulations that $\tan\delta_s$ variations (in the studied space) does not alter the e.m. field configuration, thus, for the evaluation of G and η, $\tan\delta_s$ is fixed (i.e. $\tan\delta_s = 10^{-2}$). Both $u(G)$ and $u(\eta)$ are obtained with Monte Carlo e.m. simulations randomly varying all the physical dimensions and the e.m. properties of the materials, of which the resonator is made, in their uncertainty space [24].

It should be noticed that $u(Q)/Q$ is ideally constant for every Q value if the measurement frequency span is kept proportional to f_0/Q and the number of points constant [25]. Actually, because of the mounting repeatability limitation, the presence of other resonance modes and other non idealities (e.g. a complex background signal on the transmission parameter and a cross-coupling contribution), $u(Q)$ is somehow limited even at low Q, thus its absolute value is assumed constant $u(Q) \sim 40$. In Figure 3 $u(\tan\delta_s)/\tan\delta_s$ is evaluated in the plane$(\varepsilon', \tan\delta)$ and it is reported for samples with $t = 1.5$ mm and $t = 0.5$ mm. $u(\tan\delta_s)/\tan\delta_s$ strongly depends on the sample thickness t, thus on η_s, as expected from Figure 2. $u(\tan\delta_s)$ sharply increases with thinner samples particularly at low $\tan\delta_s$ values: with $\tan\delta_s \sim 10^{-2}$ and $\varepsilon_s' \sim 2$, $u(\tan\delta_s)/\tan\delta_s \sim 100\,\%$ for a 0.5 mm thick sample while $u(\tan\delta_s)/\tan\delta_s \sim 10\,\%$ in the same conditions but with t =1.5 mm. In Figure 3 we reported also the $\varepsilon_s'(\tan\delta_s)$ curve corresponding to $|c|_{max}$: it fairly agrees with the lowest $u(\tan\delta_s)/\tan\delta_s$ level.

Once the maximum $u(\tan\delta_s)$ threshold level is fixed, from Figure 3 the space $(\varepsilon', \tan\delta)$ where the proposed technique can be reliably used is defined. However, two other limiting factors must be considered. The first is related to the impossibility to discriminate small $\Delta Q \sim Q_A - Q_S$ variations because of the measurement noise. Thus, where $\Delta Q < \Delta Q_{min}$ this technique is no more sensitive. In our case with $Q_A \sim 5000$, $\Delta Q_{min} \sim 40$. We reported in Figure 3 the ΔQ_{min} curve which however crosses the $(\varepsilon', \tan\delta)$ plane where $u(\tan\delta_s)/\tan\delta_s > 100\,\%$. The second limit is set where the losses of the sample are so high to make Q_s too small to be reliably measured. Due to the $S_{12}(f)$ background we set this minimum value $\min(Q_s) \sim 100$. In Figure 3 the dotted line represents this limit: above this curve no $\tan\delta_s$ measurements are possible.

Since we expect for 3D-printer materials $2.5 < \varepsilon_s' < 3.5$ and $5 \times 10^{-3} < \tan\delta_s < 5 \times 10^{-2}$, it is possible to exploit the minimum $u(\tan\delta_s)/\tan\delta_s$ area of the presented technique with a correct η_s tuning.

Table 1. The mean thickness $\bar{t}$ of the samples and its standard deviation σ_t.

	S_1	S_2	S_3	S_4
$\bar{t}$ (mm)	0.522	1.002	1.512	2.063
σ_t (mm)	0.003	0.004	0.005	0.004

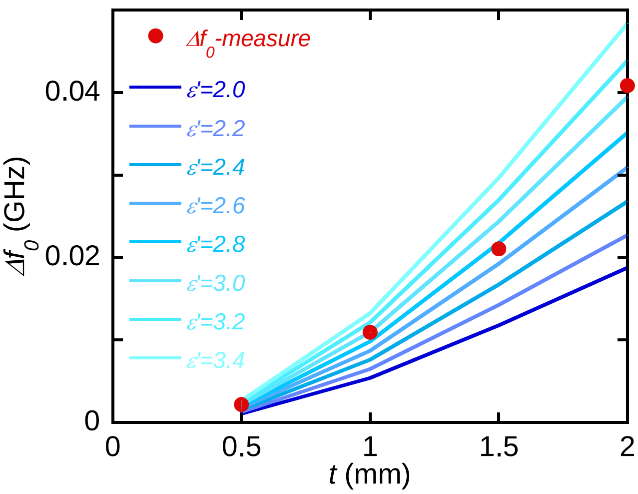

Figure 4. Differences between the resonant frequencies $f_{0,S}$ whit the samples mounted and $f_{0,A}$ whit the sample substituted by an air gap of the same thickness. The red dots are the experimental data and the blue lines the simulations results.

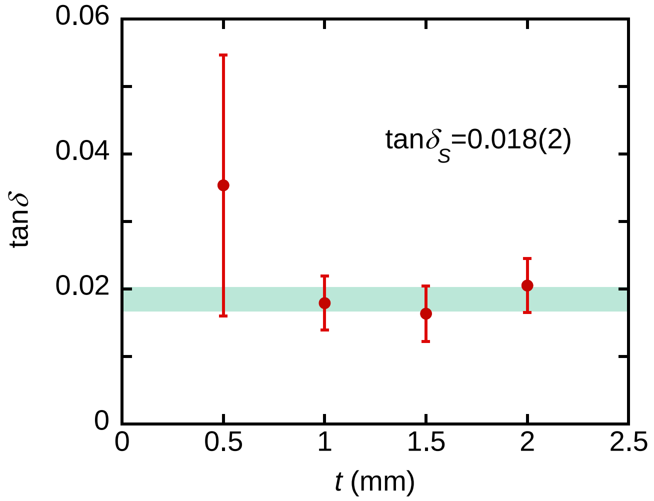

Figure 5. The measured loss tangent of the dielectric 3D-printed material $tan\,\delta_S$. The error bars are evaluated with Eq.(9) and the green area represent the confidence interval.

4. RESULTS AND DISCUSSION

The measurements were performed on four dielectric samples, made of a photopolymer material printed with PolyJet™ deposition technique, and of different thickness values t as reported in Table 1. The thickness of the samples and their flatness were checked with a micrometer. The mean values $\bar{t}$ and their standard deviation $\sigma_t = \sqrt{\sum_{i=1}^{N}(t-\bar{t})^2/(N-1)}$ have been obtained by $N = 10$ different measurements of the thickness probing the surfaces of the samples. Thus, σ_t can be read as a measure of the flatness of the samples.

A sensitive enough method to evaluate ε' relies on the frequency repeatability of our setup, so that we can reliably measure the differences between $f_{0,S}$ measured with the dielectric samples mounted and $f_{0,A}$ measured without the sample and leaving an air gap of the same sample thickness. This is done thanks to 3D-printed rings, prepared in the same way and of the same thickness of the dielectric samples. The data are presented in Figure 4: from those one can then evaluate $\varepsilon'_S = 2.9 \pm 0.2$.

Once ε'_S is estimated with its uncertainty, the geometrical and filling factors of the resonator components (with their uncertainties) are evaluated from the simulations as shown in the previous section.

Then, $\tan\delta_S$ is evaluated through Eq. (6) from the measured $\Delta(Q^{-1}) = Q_S^{-1} - Q_A^{-1}$. The quality factors Q are reported in Table 2.

In Figure 5 the measured $\tan\delta_S$ is shown with the error bars evaluated with Eq. (9) using the uncertainties on the measured quantities and simulated parameter shown previously. Figure 5 shows the best estimate: $\tan\delta_S = (1.8 \pm 0.2)\cdot 10^{-2}$ as calculated with $\varepsilon'_S = 2.9 \pm 0.2$. The evaluation of $\tan\delta_S$ is performed taking as best value the centre point in the common confidence interval of all the experimental points (the green band in Figure 5). Then, the uncertainty is the half width of that common interval. We note that the uncertainty bars rapidly increase when the sample thickness becomes small due to a lack of sensitivity as expected from the analysis presented in Sec. 3. This effect is present also in Figure 4, where the simulated curves for small thickness values tend to coalesce. On the contrary, samples with large thickness could cause e.m. field radiation from the structure, thus changing significantly the resonant mode and adding further losses. The method here presented, in our geometry, is then most suitable for samples of thickness between 1 and 2 mm.

Table 2. The inverse of the measured quality factors when the four samples, S1-S4, are inserted. $Q_S^{-1}$and Q_A^{-1} refer to the measurement with the sample and an air gap of equal thickness, respectively.

	S_1	S_2	S_3	S_4
$Q_S^{-1}\cdot 10^4$	2.15	2.48	3.06	4.25
$Q_A^{-1}\cdot 10^4$	1.95	1.96	1.98	2.00

5. COMPARISON WITH OTHER METHODS

With a combined technique, a broad band (1 MHz÷11 GHz) characterization of 3D-printer materials was presented in [13]. The high frequency range (8.2 GHz÷11 GHz) was studied through a waveguide in reflection mode, although an uncertainty study was lacking in this frequency range. Reported values at 11 GHz were $2.5 < \varepsilon' < 3.29$ and $0.005 < \tan\delta < 0.037$, perfectly in agreement with our results.

In order to check the accuracy of the DR technique shown in this paper, we measured $\tilde{\varepsilon}$ of the dielectric material here used with a standard reflection/transmission method. We used a WR90 waveguide with a PNA Network Analyzer, model E8363C, Agilent Technologies, with the Agilent 85071E software and the 'NIST precision' method [26]. To perform this measurement, we printed parallelepipeds of section $22.8\cdot 10.1$ mm² and different thickness (4, 5, 6, 7, 8 mm). We obtained $\varepsilon'_S \sim 3.1$ extrapolating the value at 12.9 GHz and no significative sample variations (Figure 6). This value is well comparable with the one obtained with the proposed DR technique using the f_0 variation.

Then, for the imaginary part we obtained $\varepsilon''_S \sim 0.23$ with the waveguide method, which yields $\tan\delta_S \sim 0.074$ and with a significative inter-sample scattering. This value is about 4 times larger than the one obtained with the DR method. However, it must be mentioned that the 'NIST precision' method was developed to solve the accuracy problems of the

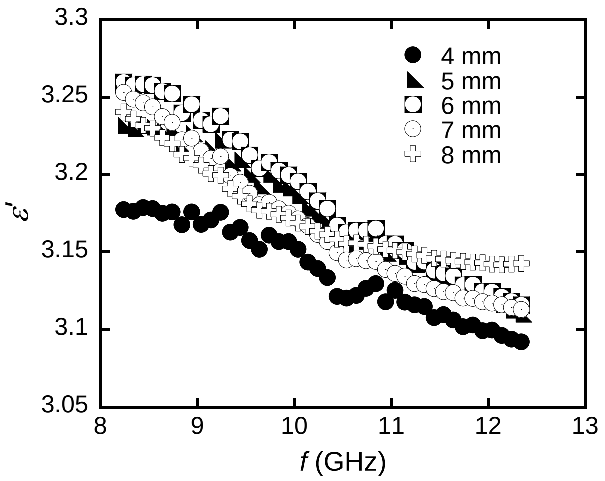

Figure 6. Real part of the complex permittivity $\Re\{\tilde{\varepsilon}\} = \varepsilon'$ measured on different thickness dielectric samples using the 'NIST precision' transmission/reflection method [26] through a WR90 waveguide.

Nicholson-Ross-Weir (NRW) technique near the sample resonances [14, 26]. The 'NIST precision' and the NRW give comparable results out of the resonances. It is well known that the NRW is not a reliable method for ε'' evaluation of low loss materials. In fact, we tested the same measurement fixture with a Polytetrafluoroethylene (PTFE) sample obtaining $\varepsilon''_{PTFE} \sim 1.5 \times 10^{-2}$, while from literature [27] it is expected to be about two order of magnitude smaller. Also for materials with higher losses, the NRW accuracy is limited: the comparison presented in [28] between the NRW and other methods shows some discrepancy even at $\tan\delta \sim 10^{-2}$ values (e.g. with nylon samples) as in our case. Thus, the incompatibility between the DR $\tan\delta$ measurement with that obtained in waveguide, will be subject of study in further works but it was something somehow expected.

6. SUMMARY

We presented a dielectric loaded-resonator-based technique for the measurement of the complex permittivity $\tilde{\varepsilon}$ of 3D printable materials. We exploited the possibility to shape the sample in appropriate shapes (disks, in our case) and the excellent frequency repeatability of our setup in order to reliably measure the quality factor Q and the resonance frequency f_0, with and without the sample loaded into the cavity. From the variations of Q and f_0 given by the sample insertion, $\tilde{\varepsilon}$ is obtained with the perturbation approach. The measurement technique performances were deeply analysed in terms of sensitivity and accuracy in the whole parameters space in order to establish the sample geometry, as a function of its e.m. properties, for the best measurement accuracy.

We tested the technique measuring photopolymer material printed with PolyJet™ deposition. We obtained $\varepsilon'_S = 2.9 \pm 0.2$ and $\tan\delta_s = 0.018 \pm 0.002$. The accuracy of the measured ε'_S was checked using the 'NIST precision' method [26] based on transmission/reflection measurements with a WR90 waveguide. The results obtained with the presented technique, both on ε'_s and $\tan\delta_s$, are fairly in agreement with other literature works.

Summarizing, we presented a new measurement technique for the e.m. characterization of dielectric materials, with interesting possible industrial applicability due to its simple conceptual approach and good accuracy.

REFERENCES

[1] N. Hopkinson, P. Dickens, Emerging rapid manufacturing processes, in Rapid Manufacturing; an Industrial Revolution for the Digital Age, N. Hopkinson, R. Hague, P. Dickens, Wiley&Sons Ltd, Chichester, 2006, ISBN: 0-470-01613-2, pp 55-80.

[2] M. J. Werkheiser, J. Dunn, M. P. Snyder, J. Edmunson, K. Cooper, M. M. Johnston, 3D printing in zero-g ISS technology demonstration., AIAA SPACE 2014 Conference and Exposition, San Diego, California, 2014, pp 2054-2078.

[3] J. Y. Wong, Ultra-portable solar-powered 3D printers for onsite manufacturing of medical resources, Aerospace Medicine and Human Performance, vol. 89, (2015), pp. 830-834.

[4] C. Schubert, M. C. Van Langeveld, L. A. Donoso, Innovations in 3D printing: a 3D overview from optics to organs, British Journal of Ophthalmology, vol. 98, (2014), pp. 159-161.

[5] F. Rengier, A. Mehndiratta, H. Von Tengg-Kobligk, C. M. Zechmann, R. Unterhinninghofen, H. Kauczor, F. L. Giesel, 3D printing based on imaging data: review of medical applications, International Journal of Computer Assisted Radiology and Surgery, vol. 5, (2010), pp. 335-341.

[6] M. J. Burfeindt, T. J. Colgan, R. O. Mays, J. D. Shea, N. Behdad, B. D. Van Veen, S. C. Hagness, MRI-derived 3-D-printed breast phantom for microwave breast imaging validation., IEEE Antennas and Wireless Propagation Letters, vol. 11, (2012), pp. 1610-1613.

[7] A. T. Mobashsher, A. M. Abbosh, Three-dimensional human head phantom with realistic electrical properties and anatomy. IEEE Antennas and Wireless Propagation Letters, vol. 13, (2014), pp. 1401-1404.

[8] A. Bisognin, A. Cihangir, C. Luxey, G Jacquemod, R. Pilard, F Gianesello, W. G. Whittow, Ball grid array-module with integrated shaped lens for WiGig applications in eyewear devices, IEEE Transactions on Antennas and Propagation, vol. 64, (2016), pp. 872-882.

[9] G. P. Le Sage, 3D printed waveguide slot array antennas, IEEE Access, vol. 4, (2016), pp. 1258-1265.

[10] A. Rashidian, L. Shafai, M. Sobocinski, J. Peräntie, J., Juuti, H. Jantunen, Printable planar dielectric antennas, IEEE Transactions on Antennas and Propagation, vol. 64, (2016), pp. 403-413.

[11] P. Nayeri, M Liang, R. A. Sabory-Garcı, M. Tuo, F. Yang, M. Gehm, A. Z. Elsherbeni, 3D printed dielectric reflectarrays: low-cost high-gain antennas at sub-millimeter waves. IEEE Transactions on Antennas and Propagation, vol. 62, (2014), pp. 2000-2008.

[12] C. R. Garcia, R. C. Rumpf, H. H. Tsang, J. H. Barton, Effects of extreme surface roughness on 3D printed horn antenna. Electronics Letters, vol. 49, (2013), pp. 734-736,

[13] P. I. Deffenbaugh, R. C. Rumpf e K. H. Church, Broadband microwave frequency characterization of 3-D printed materials, IEEE Transactions on Components, Packaging and Manufacturing Technology, vol. 3, (2013), pp. 2147-2155.

[14] L. F. Chen, C. K. Ong, C. P. Neo, V. V. Varadan and V. K. Varadan, Microwave Electronics: Measurement and Materials Characterization., John Wiley & Sons, Chichester, 2004, ISBN: 0-470-84492-2.

[15] J. Mazierska, C. Wilker, Accuracy issues in surface resistance measurements of high temperature superconductors using dielectric resonators (corrected). IEEE Transactions on Applied Superconductivity, vol. 11, (2001), pp. 4140-4147.

[16] J. Mazierska, M. V. Jacob, How accurately can the surface resistance of various superconducting films be measured with the sapphire Hakki–Coleman dielectric resonator technique?. Journal of Superconductivity and Novel Magnetism, vol. 19, (2006), pp. 649-655.

[17] J. M. Felício, C. A. Fernandes, J. R. Costa, Complex permittivity and anisotropy measurement of 3D-printed PLA at microwaves and millimeter-waves, 22nd International Conference on Applied Electromagnetics and Communications (ICECOM), Dubrovnik, Croatia, 2016, pp. 54-60.

[18] F. Castles, D. Isakov, A. Lui, Q. Lei, C. E. J. Dancer, Y. Wang, J. M. Janurudin, S. C. Speller, C. R. M. Grovenor e P. S. Grant, Microwave dielectric characterisation of 3D-printed BaTiO3/ABS polymer composites, Scientific Reports, vol. 6, 2016, art. no. 22714

[19] B. W. Hakki, P. D. & Coleman, A dielectric resonator method of measuring inductive capacities in the millimeter range, IRE Transactions on Microwave Theory and Techniques, vol. 8, (1960), pp. 402-410.

[20] JCGM 100: Evaluation of Measurement Data – Guide to the Expression of Uncertainty in Measurement, 2008.

[21] K. Torokhtii, A. Alimenti, N. Pompeo, F. Leccese, F. Orsini, A. Scorza, S. A. Sciuto, E. Silva, Q-factor of microwave resonators: calibrated vs. uncalibrated measurements, Journal of Physics: Conference Series, Vol. 1065, (2018), art. no. 052027.

[22] K. Leong, J. Mazierska, Precise measurements of the Q factor of dielectric resonators in the transmission mode-accounting for noise, crosstalk, delay of uncalibrated lines, coupling loss, and coupling reactance. IEEE Transactions on Microwave Theory and Techniques, vol. 50, (2002), pp. 2115-2127.

[23] N. Pompeo, K. Torokhtii, F. Leccese, A. Scorza, A. S. Sciuto, E. Silva, Fitting strategy of resonance curves from microwave resonators with non-idealities, IEEE International Instrumentation and Measurement Technology Conference (I2MTC), Torino, Italy, 2017, pp. 1-6.

[24] JCGM 101: Evaluation of Measurement Data – Supplement 1 to the "Guide to the Expression of Uncertainty in Measurement" – Propagation of distributions using a Monte Carlo method, 2008.

[25] K. Torokhtii, A. Alimenti, N. Pompeo, E. Silva, Uncertainty in uncalibrated microwave resonant measurements, Proceedings of the 23rd IMEKO TC4 International Symposium Electrical & Electronic Measurements Promote Industry 4.0, Xi'An, China, 2019, pp.98-101.

[26] J. Baker-Jarvis, E. J. Vanzura, W. A. Kissick,. Improved technique for determining complex permittivity with the transmission/reflection method. IEEE Transactions on microwave theory and techniques, vol. 38, (1990), pp. 1096-1103.

[27] J. Krupka, Measurements of the complex permittivity of low loss polymers at frequency range from 5 GHz to 50 GHz. IEEE Microwave and Wireless Components Letters, vol. 26, (2016), pp. 464-466.

[28] Z. Abbas, R. D. Pollard, R. W. Kelsall, R. W., Complex permittivity measurements at Ka-band using rectangular dielectric waveguide. IEEE Transactions on Instrumentation and Measurement, vol. 50, (2001), pp. 1334-1342.